THE MORTAR EDGE ELEMENT METHOD IN THREE DIMENSIONS: APPLICATION TO MAGNETOSTATICS

F. BOUILLAULT*, A. BUFFA†, Y. MADAY‡, AND F. RAPETTI§

Abstract. The subject presented in this paper concerns the approximation of a magnetostatic problem, where the primary unknown is the *magnetic vector potential* in a three-dimensional system composed of two solid parts separated by an interface. The approximation of the problem here is based on the *mortar element method* combined with edge elements on tetrahedrical meshes that do not match at the interface. In this paper we describe the proposed method and its implementation aspects together with some numerical results that illustrate how the method works.

Key words. domain decomposition method, edge element approximation, magnetostatics, mortar element method, non-matching grids

AMS subject classifications. 65M55, 68U20, 78A30, 35Q60

Introduction. The flexibily and performance of a numerical method for the simulation of electromagnetic field distributions in electrotechnical devices relies, in several cases, on the possibility of working with non-matching grids at the interface between adjacent sub-domains. One example is given by the treatment of moving structures. We can choose to work in Eulerian coordinates, adding a convective term in the equations or in Lagrangian coordinates, dealing with non-conforming discretizations. The second choice may be less expensive from the computational point of view if we use a method that avoids re-meshing or interpolation procedures. Another example is the optimization of the structure shape. We can re-mesh either the whole domain or only a region containing the shape to be optimized: in the second case it can be useful to work with non-matching grids to simplify the local re-meshing task and successive solution of the problem. A third example consists in the possibility of coupling variational methods of different orders and types.

In this paper we deal with the edge element approximation on non-matching grids of a given magnetostatic problem in three dimensions. We will focus our attention on the description of the magnetic field distribution in a domain composed of two solid parts separated by an interface. We aim at describing the three-dimensional *mortar edge element method* and its main implementation aspects.

The general problem of dealing with non-matching grids in magneto-mechanical applications has been faced for a long time (see [15, 26, 22, 14, 18, 16, 28, 29] for the main arguments that have been proposed since the 1980 and [25] for further references on the subject). None of the existing methods is simultaneously characterized by involving positive definite matrices, avoiding re-meshing and difficult intersection procedures, imposing no constraint between the discretization parameters in adjacent sub-domains.

* Laboratoire de Génie Electrique de Paris, U.M.R. 8507 C.N.R.S., Plateau de Moulon, 91192 Gif-Sur-Yvette, France. E-mail: bouillault@lgep.supelec.fr.

†Department of Mathematics, University of Pavia, Via Ferrata 1, 27100 Pavia, Italy. E-mail: annalisa@dimat.unipv.it.

‡Laboratoire d'Analyse Numérique, Paris VI University, 4 place Jussieu, 75252 Paris, France. E-mail: maday@ann.jussieu.fr.

§Laboratoire des Applications Scientifiques du Calcul Intensif, U.P.R. 9029 C.N.R.S., Building 506, Paris XI University, 91403 Orsay, France E-mail: rapetti@asci.fr. This work has been finantied by the European Community (TMR Contract ERB4001GT965424) and by C.N.R.S..

The mortar element method was firstly introduced in [5] in the context of Lagrangian finite elements and spectral approximation for two-dimensional elliptic partial differential equations. This method is a non-conforming non-overlapping domain decomposition technique which allows for independent (and thus, in general, non-matching at the interface) meshes in adjacent sub-domains. The idea of the mortar method is to weakly impose the transmission conditions at the interfaces by means of Lagrangian multipliers which are chosen in a suitable sub-space of the space of traces of the finite elements considered in one of the two adjacent subdomains. In the context of edge elements approximation for three dimensional Maxwell equations, the mortar method was recently introduced in [3], and its convergence analyzed from the mathematical point of view. The choice of Lagrange multipliers which is analyzed in [3] is different from the ones proposed in [17, 18, 16, 28].

In the present paper, we apply the mortar edge element method for the numerical approximation of the magnetostatic problem; the magnetic vector potential is chosen as primary variable. The magnetic vector potential formulation is widely used in electromagnetic field computation due to its robustness [1, 6, 7]. However, in this formulation, there are two essential problems: the uniqueness and the compatibility. Uniqueness can be achieved by imposing a gauge condition and the compatibility of the **curl**-**curl** equation is insured when the right hand side (the current density) is divergence free.

Our choice of dealing with a particular magnetostatic problem in a given non-moving structure is related to the following considerations. First, we want to test the reliability and the actual convergence property of the mortar edge element method in three dimensions. Second, already with still geometries and non-matching grids, we have to face, from the implementation point of view, the main difficulties we will face with moving structures and in more complex situations as, for example, in presence of curved interface between adjacent sub-domains.

Concerning the paper organization, in Section 1 we deduce the model from the system of Maxwell's equations and we write the variational formulation of the problem. To satisfy the compatibility and uniqueness conditions on the magnetic vector potential, we adopt an approach similar to the one presented in [27]. The compatibility is ensured expressing the current density by the curl of a source field and projecting this source field in the space $\mathbf{curl}(\mathcal{P})$, where $\mathcal{P}$ is a suitable space of edge elements [7, 20, 21]. Then, by using the Conjugate Gradient algorithm to solve the final algebraic system, uniqueness is achieved in the space orthogonal to $\ker(\mathbf{curl})$. In Section 2 we discuss the spatial discretization by introducing the mortar edge element method and we present some of the implementation features of the method. In Section 3 we describe the discretization of the coupling condition, ending, in Section 4, with the presentation of some numerical results.

1. The continuous problem. In this section, we present the mathematical model of the problem we are going to study, giving three sequential formulations of it. The first formulation is classical and follows from Maxwell's equations; the second is a more appropriate version of the first one for the edge element approximation and the last formulation is the one we deal with in a domain decomposition approach.

1.1. Classical formulation. Let Ω be a Lipschitz contractible open subset of $\mathbb{R}^3$. We fix on it a system of Cartesian coordinates, say $\mathbf{x} = (x, y, z)$ and we suppose that Ω is bounded in each direction. We denote by $\mathbf{n}$ the outer normal vector to $\partial\Omega$.

The magnetostatic problem that we analyse here consists in the determination of the magnetic vector potential $\mathbf{u}$ (i.e. a vector $\mathbf{u}$ such that the magnetic induction

($\mathbf{B} = \ \mathbf{curl}\ \mathbf{u}$) solution of the following problem:

$$\text{(1)} \qquad \begin{aligned} &\mathbf{curl}\ (\nu\ \mathbf{curl}\ \mathbf{u}) = \mathbf{J} && \text{in } \Omega\,, \\ &(\mathbf{u})_{T,\partial\Omega} = \mathbf{0} && \text{on } \partial\Omega\,, \end{aligned}$$

where $(\mathbf{u})_{T,\partial\Omega} = \mathbf{n}\times(\mathbf{u}\times\mathbf{n})$ is the tangential component of $\mathbf{u}$ on $\partial\Omega$, ν is the magnetic reluctivity and $\mathbf{J}$ a prescribed current density. We assume that ν is not a tensor but a scalar function of the space variable $\mathbf{x}$.

Since we aim at using a finite element discretization, it is natural to refer to the variational formulation of problem (1). Let us introduce the space

$$H_0(\mathbf{curl},\Omega) = \{\mathbf{u} \in L^2(\Omega)^3 \,|\, \mathbf{curl}\ \mathbf{u} \in L^2(\Omega)^3 \text{ and } (\mathbf{u})_{T,\partial\Omega} = \mathbf{0}\,\}\,.$$

It is classical to notice that solving (1) in $H_0(\mathbf{curl},\Omega)$ for current densities $\mathbf{J}$ in $(H_0(\mathbf{curl},\Omega))'$ is equivalent to solve the following variational problem:

$$\text{(2)} \qquad \begin{aligned} &\text{Given } \mathbf{J} \in (H_0(\mathbf{curl},\Omega))'\,, \ \text{ find } \mathbf{u} \in H_0(\mathbf{curl},\Omega) \text{ such that:} \\ &\quad \int_\Omega \nu\ \mathbf{curl}\,\mathbf{u}\cdot\ \mathbf{curl}\,\mathbf{v}\, d\Omega = \int_\Omega \mathbf{J}\cdot\mathbf{v}\, d\Omega\ , \qquad \forall \mathbf{v} \in H_0(\mathbf{curl},\Omega)\,. \end{aligned}$$

The existence of solutions to the problem is standard (see [7]); the difficulty is at the level of uniqueness since the solution is determined up to the gradient of a scalar function. An additional constraint must be imposed in order to ensure the uniqueness of the vector potential $\mathbf{u}$.

A standard approach is to add a jauge condition as explained in [13, 1]. But this is not the only way to achieve uniqueness, as it is explained at the discrete level in what follows. Discretized the physical domain Ω by a mesh and introduced a finite element space Y_h of dimension n as a finite dimensional approximation of $H_0(\mathbf{curl},\Omega)$, the matrix form of problem (2) is given by

$$\text{(3)} \qquad M\mathbf{U} = \mathbf{F}$$

where M is a symmetric, non-negative matrix of dimension n, $\mathbf{U}$ is the vector of degrees of freedom of $\mathbf{u}$ in the chosen space Y_h when $\mathbf{F}$ is associated to the right-hand side of the discrete version of problem (2). We remark that

$$\ker(M) = \{\mathbf{U} \in \mathbb{R}^n \,|\, M\mathbf{U} = \mathbf{0}\} \neq \{0\}\,,$$

i.e. the **curl**-**curl** matrix M is singular. Nevertheless, in what follows we note that system (3) is uniquely solvable in $\ker(M)^\perp = \{\mathbf{U} \in \mathbb{R}^n | \mathbf{U}\cdot\mathbf{Y} = 0, \forall\mathbf{Y} \in \ker(M)\}$ if it is compatible, i.e. $\mathbf{F} \in \mathrm{range}(M) = \{M\mathbf{U} \,|\, \mathbf{U} \in \mathbb{R}^n\}$. Moreover, being M symmetric, we have that $\mathrm{range}(M) = \ker(M)^\perp$.

To solve (2), we start by introducing a source field $\mathbf{T}$, such that

$$\text{(4)} \qquad \mathbf{J} = \ \mathbf{curl}\ \mathbf{T} \quad \text{in } \Omega \quad \text{and} \quad (\mathbf{T})_{T,\partial\Omega} = \mathbf{0} \quad \text{on } \partial\Omega\,.$$

We replace $\mathbf{J}$ by $\mathbf{curl}\ \mathbf{T}$ in (2) and we integrate by parts. The variational problem we solve is then:

$$\text{(5)} \qquad \begin{aligned} &\text{Given } \mathbf{T} \in L^2(\Omega)^3\,, \ \text{ find } \mathbf{u} \in H_0(\mathbf{curl},\Omega) \text{ such that} \\ &\int_\Omega \nu\ \mathbf{curl}\ \mathbf{u}\cdot\mathbf{curl}\ \mathbf{v}\, d\Omega = \int_\Omega \mathbf{T}\cdot\mathbf{curl}\ \mathbf{v}\, d\Omega\ , \qquad \forall \mathbf{v} \in H_0(\mathbf{curl},\Omega) \end{aligned}$$

and its matrix form is $M\mathbf{U}' = \mathbf{F}'$, where $\mathbf{U}'$ is the vector of degrees of freedom of $\mathbf{u}$ when $\mathbf{F}'$ is associated to the right-hand side of the discrete version of problem (5). The right-hand side $\mathbf{F}' \in \ker(M)^{\perp} (= \mathrm{range}(M))$ *by construction* and the compatibility condition is fulfilled. If we solve $M\mathbf{U}' = \mathbf{F}'$ by the Conjugate Gradient, we have

$$\mathbf{U}'_{k+1} = \mathbf{U}'_k + \alpha_k \mathbf{p}_k \tag{6}$$

where α_k is the iterative coefficient and $\mathbf{p}_k$ the conjugate vector of M, which can be expressed as a linear combinations of the residuals at the previous iterations, i.e. $\mathbf{p}_k = \sum_{i\leq k} c_i\,(M\mathbf{U}' - \mathbf{F}')$. It appears that $\mathbf{p}_k \in \mathrm{range}(M) = \ker(M)^{\perp}$, we thus have $\mathbf{U}'_{k+1} \in \ker(M)^{\perp}$. These considerations are still valid in a domain decomposition approach.

REMARK 1.1. *In presence of inductors with simply-shaped geometry (as the ones we will consider in Section 4), the vector* $\mathbf{T}$ *can be analytically computed.*

In more general situations, to fulfill the compatibility condition, the density current $\mathbf{J}$ *has to be discretized by suitable* $H(div,\Omega)$*-conforming finite elements, where* $H(div,\Omega) = \{\mathbf{u} \in L^2(\Omega)^3 \mid div\ \mathbf{u} \in L^2(\Omega)\}$*. Another possibility is to solve the following problem:*

$$\begin{aligned} &\textit{Given } \mathbf{J} \in (H_0(\mathbf{curl},\Omega))',\ \textit{find } \mathbf{T} \in H_0(\mathbf{curl},\Omega) \textit{ such that} \\ &\textstyle\int_\Omega \mathbf{curl}\ \mathbf{T} \cdot \mathbf{curl}\ \mathbf{T}'\, d\Omega = \int_\Omega \mathbf{J} \cdot \mathbf{curl}\ \mathbf{T}'\, d\Omega\ , \quad \forall \mathbf{T}' \in H_0(\mathbf{curl},\Omega)\,, \end{aligned} \tag{7}$$

that is the weak form of problem (4), in the same way we solved (5). In this case, the determination of the source vector $\mathbf{T}$ *seems to be of the same complexity as the one of the magnetic vector potential* $\mathbf{u}$*. But in contrast to what happens for* $\mathbf{u}$*, vector* $\mathbf{T}$ *is not influenced by jumps in the reluctivity* ν *and its determination is less expensive since it is needed only in a part of the computational domain* Ω *containing the conductors (and it is then extended by zero to the full domain* Ω*).*

We have also to remark that, equation $\mathbf{curl}\,(\nu\ \mathbf{curl}\ \mathbf{u}) = \mathbf{J}$ *is compatible if* $div\ \mathbf{J} = 0$*. In concrete situations, the source current (either supplied by generators or computed by solving a circuit equation) can loose its divergence-free character: expressing* $\mathbf{J}$ *as the curl of a source field* $\mathbf{T}$ *is a way to re-establish this feature, before running numerical simulations.*

1.2. Domain decomposition approach. The first step in the application of a domain decomposition method to solve (5) consists in dividing the considered domain into a finite number of sub-domains. In the considered case, we divide Ω into at least two sub-domains separated by an interface, as represented in Figure 1 for example. We thus have $\overline{\Omega} = \overline{\Omega_1} \cup \overline{\Omega_2}$ and the interface $\Gamma = \overline{\Omega_1} \cap \overline{\Omega_2}$. We denote by $\mathbf{n}_\Gamma$ the unit normal vector to Γ, directed from Ω_1 to Ω_2.

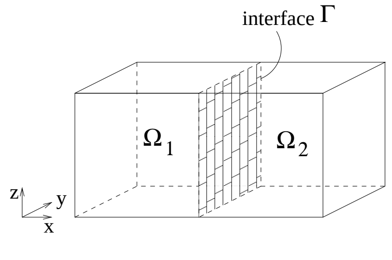

FIG. 1. *The domain* Ω*: a flat interface separates* Ω_1 *from* Ω_2*.*

The second step consists in re-writing problem (5) in a transmission form. To this aim, we split the integral over Ω in a sum of integrals over the sub-domains Ω_k

(k = 1,2 in our case) and the solution is sought for a pair $(\mathbf{u}_1, \mathbf{u}_2)$ where $\mathbf{u}_k$ is the restriction of $\mathbf{u}$ to Ω_k. Note that only a transmission condition (of Dirichlet type) has to be explicitly enforced on both the solution and the test functions in order to get a problem equivalent to (5). Recalling the standard result that the tangential component of a function in $H(\mathbf{curl}, \Omega)$ is continuous and belongs to $H^{-\frac{1}{2}}(\partial\Omega)^2$, we are led to introduce the following functional space:

$$\mathcal{U} = \{(\mathbf{u}_1, \mathbf{u}_2) \in H(\mathbf{curl}, \Omega_1) \times H(\mathbf{curl}, \Omega_2) \mid (\mathbf{u}_1)_{T,\Gamma} = (\mathbf{u}_2)_{T,\Gamma}\}, \tag{8}$$

with $H(\mathbf{curl}, \Omega_k) = \{\mathbf{u} \in L^2(\Omega_k)^3 \mid \mathbf{curl}\ \mathbf{u} \in L^2(\Omega_k)^3\}$. We recall that $(\mathbf{u})_{T,\Gamma} = \mathbf{n}_\Gamma \wedge (\mathbf{u} \wedge \mathbf{n}_\Gamma)$ is the tangential component of $\mathbf{u}$ on Γ.

We remark that $\mathcal{U}$ is a closed subspace of $H(\mathbf{curl}, \Omega_1) \times H(\mathbf{curl}, \Omega_2)$ and so an Hilbert space with the natural norm (usually called broken norm)

$$||\mathbf{u}||_\star^2 = ||\mathbf{u}_1||^2_{H(\mathbf{curl},\Omega_1)} + ||\mathbf{u}_2||^2_{H(\mathbf{curl},\Omega_2)}. \tag{9}$$

where $||\mathbf{u}||^2_{H(\mathbf{curl},\Omega_k)} = ||\mathbf{u}||^2_{L^2(\Omega_k)^3} + ||\ \mathbf{curl}\ \mathbf{u}||^2_{L^2(\Omega_k)^3}$. It can be proven that the mapping $\mathbf{u} \to (\mathbf{u}_1 = \mathbf{u}_{|\Omega_1}, \mathbf{u}_2 = \mathbf{u}_{|\Omega_2})$ is an isomorphism between $H(\mathbf{curl}, \Omega)$ and $\mathcal{U}$. We denote by $\mathcal{U}^0 = \{(\mathbf{u}_1, \mathbf{u}_2) \in \mathcal{U} \mid (\mathbf{u}_k)_{T,\partial\Omega_k\cap\partial\Omega} = \mathbf{0}\,,\ k = 1,2\}$; this space is associated to $H_0(\mathbf{curl}, \Omega)$ through the previous isomorphism. By classical reasoning we obtain the following variational formulation, to be intended in the sense of distributions:

Given $(\mathbf{T}_1, \mathbf{T}_2) \in L^2(\Omega_1)^3 \times L^2(\Omega_2)^3$, find $(\mathbf{u}_1, \mathbf{u}_2) \in \mathcal{U}^0$ such that :

$$\sum_{k=1}^{2} \int_{\Omega_k} \nu\, \mathbf{curl}\ \mathbf{u}_k \cdot\ \mathbf{curl}\ \mathbf{v}_k\, d\mathbf{x} = \sum_{k=1}^{2} \int_{\Omega_k} \mathbf{T}_k \cdot\ \mathbf{curl}\ \mathbf{v}_k\, d\mathbf{x}\,,\ \forall(\mathbf{v}_1, \mathbf{v}_2) \in \mathcal{U}^0\,. \tag{10}$$

Any solution of (10) satisfies, in the sense of distributions,

$$\begin{array}{lll} (E_k) & \mathbf{curl}\ (\nu\ \mathbf{curl}\ \mathbf{u}_k) = \mathbf{J}_{|\Omega_k} & \text{in } \Omega_k \quad , \quad k = 1,2 \\ (BC_k) & (\mathbf{u}_k)_{T,\partial\Omega_k\cap\partial\Omega} = \mathbf{0} & \text{on } \partial\Omega_k \cap \partial\Omega \quad , \quad k = 1,2\,. \end{array}$$

To have a problem equivalent to (5), $\mathbf{u}_1$ and $\mathbf{u}_2$ must satisfy the transmission condition (of Dirichlet type) on the interface Γ, that is

$$(TCD) \qquad (\mathbf{u}_1)_{T,\Gamma} = (\mathbf{u}_2)_{T,\Gamma} \quad \text{on } \Gamma\,.$$

A transmission condition (of Neumann type) can be further completed by going back to the strong formulation of the problem. In fact, by integrating by parts the equation (10) we derive in a weak sense (duality with the space of tangential components of functions in $H(\mathbf{curl}, \Omega)$) that

$$(TCN) \qquad (\nu\ \mathbf{curl}\ \mathbf{u}_1)_{T,\Gamma} = (\nu\ \mathbf{curl}\ \mathbf{u}_2)_{T,\Gamma} \quad \text{on } \Gamma\,.$$

The physical interpretation of the transmission conditions (TCD) and (TCN) is, respectively, the continuity of the normal component of the magnetic induction and of the tangential component of the magnetic field across the interface Γ.

2. The discrete problem. We now discretize (10) in each sub-domain by using edge elements. For the spatial discretization, the use of a standard conforming method, allows the transmission condition (TCD) to be exactly verified. To do this, we have to work with matching meshes at the interface Γ.

This fact can be very demanding: in presence of moving structures, for example, it is necessary to modify the mesh used for the spatial discretization at every new position of the free part or to impose a constraint between the movement characteristic entity (i.e. the rotation angle or the translation lenght) and the discretization parameter.

By using the mortar element method, we introduce a non-conforming approximation of problem (10) that allows for non-matching grids at the interface; in particular the transmission condition (TCD) is weakly imposed by means of Lagrange multipliers. This method has already been proved to be efficient in treating two-dimensional problems both combined with nodal elements (see [9, 23]) and edge ones (see [2, 24]). The method we shall describe and implement here develops what is presented in [3], where the proper space of Lagrange multipliers is defined and optimality of the approximation is proven, and [10], where a different version of the method is proposed.

2.1. Case of one domain. Let $\mathcal{T}_h$ be a family of triangulations of $\overline{\Omega}$ by means of an unstructured mesh composed of tetrahedra K such that

$$\overline{\Omega} = \bigcup_{K \in \mathcal{T}_h} K$$

with $h = \max \{ \operatorname{diam}(K)\,,\, K \in \mathcal{T}_h \}$. We assume that $\mathcal{T}_h$ is regular [12] and that its generic element K may be obtained as the image of a reference one $\hat{K}$ through an invertible affine mapping $F_K : \hat{K} \to K$, i.e. $K = \mathbf{F}_K(\hat{K})$, where $\hat{K}$ is a reference tetrahedron and $\mathbf{F}_K$ has the form

$$(11)\quad \mathbf{x} = \mathbf{F}_K(\hat{\mathbf{x}}) = B_K\,\hat{\mathbf{x}} + \mathbf{b}_K \;\;,\;\; B_K \in L(\mathbb{R}^3, \mathbb{R}^3) \;\;,\;\; \det(B_K) \neq 0 \;\;,\;\; \mathbf{b}_K \in \mathbb{R}^3$$

with B_K and $\mathbf{b}_K$ depending on K. We then introduce the finite-dimensional space

$$(12)\qquad Y_h = \{\mathbf{v}_h \in H(\mathbf{curl}, \Omega) \,|\, B_K^t(\mathbf{v}_{h\,|K} \circ F_K) \in \mathcal{P}(\hat{K})\,,\, \forall K \in \mathcal{T}_h\}$$

where ^{t} denotes the transpose operator and $\mathcal{P}(\hat{K})$ is a suitable space of polynomials on $\hat{K}$ that can be defined at least in two ways as it follows.

2.1.1. First family: six degrees of freedom per tetrahedron. A first choice for the space $\mathcal{P}(\hat{K})$ involved in (12) is given by $\mathcal{P}_1(\hat{K})$ (defined in [20])

$$\mathcal{P}_1(\hat{K}) = (\mathbb{P}_0(\hat{K}))^3 \oplus \{\mathbf{u} \in (\tilde{\mathbb{P}}_1(\hat{K}))^3 \;|\; \mathbf{u}\cdot\hat{\mathbf{x}} = 0\,,\, \forall\, \hat{\mathbf{x}} \in \hat{K}\}$$

where $\mathbb{P}_k$, $k = 0, 1$, and $\tilde{\mathbb{P}}_1$ denote the spaces of polynomials of degree $\leq k$, $k = 0, 1$, and homogeneous polynomials of degree 1, respectively. Different degrees of freedom and basis functions can be considered and in the following we detail our choice.

Given a tetrahedron K, let $\mathbf{r}_j$ (j=1,4) be the position vectors of its vertices and $\lambda_j(\mathbf{r})$ be the barycentric coordinate of a point $P \in K$ (with vector position $\mathbf{r}$) with respect to the vertex j. The vector function corresponding to an edge e_{ij}, oriented from $\mathbf{r}_i$ to $\mathbf{r}_j$, is

$$(13)\quad \mathbf{w}_{ij}(\mathbf{r}) = \lambda_i(\mathbf{r}) \operatorname{grad} \lambda_j(\mathbf{r}) - \lambda_j(\mathbf{r}) \operatorname{grad} \lambda_i(\mathbf{r}) \quad,\quad i,j = 1,2,3,4,\, i < j\,,$$

and we consider $\mathcal{P}_1(K)$ as the space generated by the basis functions settled in (13). We can define the interpolating function $\mathbf{u}_h$ on K for the vector $\mathbf{u} \in (C^0(\overline{K}))^3$ of the following form

$$\mathbf{u}_h = \sum_{i=1}^{3}\sum_{j=i+1}^{4} \mathbf{w}_{ij}\,\alpha_{ij}(\mathbf{u}) \quad \text{with} \quad \alpha_{ij}(\mathbf{u}) = |e_{ij}|\,(\mathbf{u}\cdot\mathbf{t}_{e_{ij}})(\mathbf{x}_{ij}^M) \tag{14}$$

where $|e_{ij}|$ is the length of e_{ij}, $\mathbf{x}_{ij}^M$ its midpoint and $\mathbf{t}_{e_{ij}}$ its tangent unit vector. The first family of edge elements on K is defined by $(K, \mathcal{P}_1, A)$, where A is the set of the degrees of freedom given by the linear functionals α_{ij} acting on $(C^0(\overline{K}))^3$. These finite elements belong to the Whitney's complexe [30] and coincide with the edge elements of first order defined in [20] for tetrahedra, for a suitable choice of the quadrature formula nodes to compute the associated degrees of freedom.

2.1.2. Second family: twelve degrees of freedom per tetrahedron. A second choice for the space $\mathcal{P}(\hat{K})$ involved in (12) is given by $\mathcal{P}_2(\hat{K})$ (defined in [21])

$$\mathcal{P}_2(\hat{K}) = (I\!P_1(\hat{K}))^3\,.$$

Keeping the same notations as the ones used to introduce the first family of edge elements, the vector functions corresponding to an edge e_{ij}, oriented from $\mathbf{r}_i$ to $\mathbf{r}_j$, is

$$\tilde{\mathbf{w}}_{ij}(\mathbf{r}) = \lambda_i(\mathbf{r})\ \text{grad}\ \lambda_j(\mathbf{r}) \quad , \quad i,j = 1,2,3,4,\ i \neq j\,, \tag{15}$$

and we consider $\mathcal{P}_2(K)$ as the space generated by the basis functions defined in (15). We can define the interpolating function $\mathbf{u}_h$ on K for the vector $\mathbf{u} \in (C^0(\overline{K}))^3$ of the following form

$$\mathbf{u}_h = \sum_{i=1}^{4}\sum_{j\neq i, j=1}^{4} \tilde{\mathbf{w}}_{ij}\,\beta_{ij}(\mathbf{u}) \quad \text{with} \quad \begin{array}{l} \beta_{ij}(\mathbf{u}) = |e_{ij}|\,(\mathbf{u}\cdot\mathbf{t}_{e_{ij}})(\mathbf{x}_i) \\ \beta_{ji}(\mathbf{u}) = |e_{ij}|\,(\mathbf{u}\cdot\mathbf{t}_{e_{ij}})(\mathbf{x}_j) \end{array} \tag{16}$$

where $\mathbf{x}_i$ and $\mathbf{x}_j$ are the end points of the edge e_{ij}. The second family of edge element on K is defined by $(K, \mathcal{P}_2, B)$, where B is the set of the degrees of freedom given by the linear functionals β_{ij} and β_{ji} acting on $(C^0(\overline{K}))^3$. These finite elements have been introduced by Mur and de Hoop [19] and coincide with the edge elements of first order defined in [21] for tetrahedra, for a suitable choice of the quadrature formula nodes to compute the associated degrees of freedom.

REMARK 2.1. *The basis functions are usually computed on the reference tetrahedron $\hat{K}$ as in (13) or (15) and transported on the mesh tetrahedron K through the transformation*

$$\mathbf{u}(\mathbf{x}) = (B_K^t)^{-1}\,\hat{\mathbf{u}}(F_K^{-1}(\mathbf{x}))\,. \tag{17}$$

where $\hat{\mathbf{u}}$ denotes a vector of $\mathcal{P}(\hat{K})$, $\mathbf{u}$ the corresponding vector in $\mathcal{P}(K)$ and ^{t} the transpose operator.

2.2. Case of domain decomposition. Let $\mathcal{T}_{k,h_k}$ be two families of triangulations of $\overline{\Omega}_k$ (k=1,2) by means of an unstructured mesh composed of tetrahedra K such that

$$\overline{\Omega}_k = \bigcup_{K\in\mathcal{T}_{k,h_k}} K$$

with $h_k =\ \max\ \{\ \text{diam}(K)\,,\ K \in \mathcal{T}_{k,h_k}\ \}$. We assume that they are regular and non-matching at the interface Γ. It can a priori even happen that h_1 and h_2 are different.

We aim at introducing a non-conforming finite element space, adapted to domain decomposition, for the approximation of (10). Defined

$$Y_{k,h_k} = \{\mathbf{v}_{k,h_k} \in H(\mathbf{curl},\Omega_k)\,|\,\mathbf{v}_{k,h_k\,|K} \in \mathcal{P}(K)\,,\,\forall K \in \mathcal{T}_{k,h_k}\} \tag{18}$$

where $\mathcal{P}$ corresponds to the first or second family of edge elements, we introduce

$$X_{k,h_k} = \{\mathbf{v}_{k,h_k} \in Y_{k,h_k}\,|\,(\mathbf{v}_{k,h_k})_{T,\partial\Omega_k\cap\partial\Omega} = \mathbf{0}\} \quad , \quad k = 1,2\,. \tag{19}$$

We now study the discretization of the transmission condition (TCD). When looking for a discrete counterpart of the space $\mathcal{U}$, the equality $(\mathbf{u}_1)_{T,\Gamma} = (\mathbf{u}_2)_{T,\Gamma}$ on Γ becomes a too stringent condition since both fields are defined on a-priori different and non-matching grids. As a standard procedure for non-conforming domain decomposition methods, we impose the transmission condition (TCD) in a weak form by means of a suitable space of Lagrangian multipliers M_h. We denote $h = \max(h_1, h_2)$.

We focus the attention on the interface Γ. Let $\hat{T} := \{\hat{\mathbf{x}} = (\hat{x},\hat{y}) \in I\!R^2\,,\,0 < \hat{x} < 1\,,\,0 < \hat{y} < 1 - \hat{x}\}$ be the reference triangle with edges $\hat{e}_1$, $\hat{e}_2$, $\hat{e}_3$ and outer normal $\hat{\mathbf{n}}$. We denote by $(\mathcal{T}_{k,h_k})_{|\Gamma}$ $(k = 1,2)$ the two discretizations of Γ composed of faces T belonging to tetrahedra of $\mathcal{T}_{k,h_k}$. Let

$$\begin{aligned} UK &:= \cup\{T \in (\mathcal{T}_{k,h_k})_{|\Gamma} \text{ such that } \overline{T}\cap\partial\Gamma \text{ consists in one edge of } T\,\} \\ DK &:= \cup\{T \in (\mathcal{T}_{k,h_k})_{|\Gamma} \text{ such that } \overline{T}\cap\partial\Gamma \text{ consists in two edges of } T\,\} \end{aligned}$$

Any $T \in (\mathcal{T}_{k,h_k})_{|\Gamma}$ is obtained from the reference triangle $\hat{T}$ by the linear invertible mapping $f_T : \hat{T} \to T$, $f_T(\hat{\mathbf{x}}) = B_T\hat{\mathbf{x}} + \mathbf{b}_T$, where the matrix $B_T \in I\!R^{2\times 2}$ and the constant vector $\mathbf{b}_T \in I\!R^2$. Let

$$T_h := \{(\mathbf{v}_{2,h_2})_{T,\Gamma}\,,\,\mathbf{v}_{2,h_2} \in Y_{2,h_2}\,\} \tag{20}$$

be the space of tangential components on Γ of the edge element space Y_{2,h_2}. The space T_h is $H(\mathbf{curl},\Gamma)$-conforming and it is composed of functions $\hat{\mathbf{v}} : \hat{T} \to I\!R^2$, $\hat{\mathbf{v}} \in I\!P_1(\hat{T})^2$ with degrees of freedom defined in (14) (for the first family) and in (16) (for the second family) over $\hat{e} = \hat{e}_1$, $\hat{e}_2$, $\hat{e}_3$, and defined on the current face T by means of the transformation $\mathbf{v}(\mathbf{x}) = (B_T^t)^{-1}\hat{\mathbf{v}}(\hat{\mathbf{x}})\,,\,\mathbf{x} = B_T\hat{\mathbf{x}} + \mathbf{b}_T$. We choose M_h as a proper subset of T_h, such that dim $(M_h) =$ dim $(T_h \cap H_0(\mathbf{curl},\Gamma))$. In the mortar element method terminology, this means that we choose Ω_1 as *master* and the Ω_2 as *slave*. The definition of M_h involving the edge element space Y_{1,h_1} gives a different but similar mortar method (as it is illustrated by numerical results in Figure 11).

We assume that the mapping $f_T : \hat{T} \to T$ associates to the edge $(\overline{T}\cap\partial\Gamma)$ the edge of $\hat{T}$ lying on $\{\hat{y} = 0\}$ for all $T \in UK$ and the edges of $\hat{T}$ lying on $\{\hat{y} = 0\}$ and $\{\hat{x} = 0\}$ to the edges $(\overline{T}\cap\partial\Gamma)$ for all $T \in DK$ (this is exhaustive up to a rotation, as we remark later). The space M_h is defined as follows: for the second family, as in [3]

$$\begin{aligned} M_h := \{\varphi_h \in T_h\,|\; & B_T^t(\varphi_h\circ f_T) \in I\!P_1(\hat{T})^2, && \text{if } \overline{T}\cap\partial\Gamma = \emptyset \text{ or } \{\text{one point}\}, \\ & B_T^t(\varphi_h\circ f_T) \in I\!P_0(\hat{T})\times I\!P_1(\hat{T}), && \text{if } \overline{T}\cap\partial\Gamma = \{\text{one edge}\}, \\ & B_T^t(\varphi_h\circ f_T) \in I\!P_0(\hat{T})^2, && \text{if } \overline{T}\cap\partial\Gamma = \{\text{two edges}\}\,\}. \end{aligned} \tag{21}$$

and for the first family,

$$\begin{aligned} M_h := \{\varphi_h \in T_h\,|\; & B_T^t(\varphi_h\circ f_T) \in \mathcal{P}_1(\hat{T}), && \text{if } \overline{T}\cap\partial\Gamma = \emptyset \text{ or } \{\text{one point}\}, \\ & B_T^t(\varphi_h\circ f_T) \in I\!P_0(\hat{T})^2, && \text{if } \overline{T}\cap\partial\Gamma = \{\text{one edge}\}, \\ & B_T^t(\varphi_h\circ f_T) \in I\!P_0(\hat{T})(-1,1)^t, && \text{if } \overline{T}\cap\partial\Gamma = \{\text{two edges}\}\,\} \end{aligned} \tag{22}$$

where $\mathcal{P}_1(\hat{T})$ is the two dimensional version of the space $\mathcal{P}_1(\hat{K})$. We then introduce

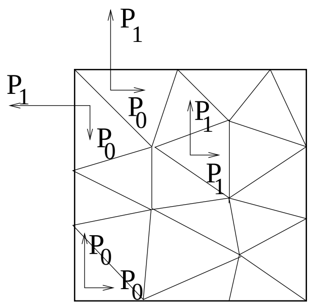

FIG. 2. *Graphical "representation" of the Lagrange multipliers on Γ: the degrees of the polynomial components of $(\varphi_h)_{|T}$ are displayed depending on the position of the triangle T on the interface.*

the approximation space:

$$\mathcal{U}_h = \{\, (\mathbf{v}_{1,h}, \mathbf{v}_{2,h}) \in X_{1,h} \times X_{2,h} \ \text{ such that } \ \forall \varphi_h \in M_h \qquad (23)$$
$$\int_\Gamma ((\mathbf{v}_{1,h})_{T,\Gamma} - (\mathbf{v}_{2,h})_{T,\Gamma}) \cdot \varphi_h \, d\Gamma = 0 \,\} \,.$$

The constraint (23) is the discrete weak version of the transmission condition (TCD). Let us introduce $\mathcal{U}_h^0 = \{(\mathbf{v}_{1,h}, \mathbf{v}_{2,h}) \in \mathcal{U}_h \mid (\mathbf{v}_{k,h})_{T,\partial\Omega_k \cap \partial\Omega} = \mathbf{0}\,,\, k = 1, 2\}$; we now look for a solution of the following variational problem:

$$\text{Find} \quad (\mathbf{u}_{1,h}, \mathbf{u}_{2,h}) \in \mathcal{U}_h^0 \ \text{ such that } \forall\, (\mathbf{v}_{1,h}, \mathbf{v}_{2,h}) \in \mathcal{U}_h^0 \ :$$
$$\sum_{k=1}^{2} \int_{\Omega_k} \nu \, \mathbf{curl}\ \mathbf{u}_{k,h} \cdot \ \mathbf{curl}\ \mathbf{v}_{k,h} \, d\mathbf{x} = \sum_{k=1}^{2} \int_{\Omega_k} \mathbf{T}_{k,h} \cdot \ \mathbf{curl}\ \mathbf{v}_{k,h} \, d\mathbf{x} \,. \qquad (24)$$

2.3. More details on the Lagrange multiplier space. Before presenting the construction of a basis for the approximation space $\mathcal{U}_h^0$ and how the condition (23) is implemented, we describe a way to compute the elements of a basis for M_h. The following descriptions are valid for both domains Ω_k $(k = 1, 2)$. Let $\hat{T}$ be the unit triangle in the plane $\{\hat{z} = 0\}$ as previously defined and $T \in (\mathcal{T}_{k,h_k})_{|\Gamma}$.

2.3.1. Description of a basis for M_h in case the second family is used.

Internal triangles – We suppose that $\overline{T} \cap \partial\Gamma = \emptyset$ (see Figure 3). The space $(M_h)_{|T}$ contains *six* functions $\varphi_h \in T_h$ with degrees of freedom defined in (16) for all the three edges. The basis functions are

$$\varphi_{ij} = (\tilde{\mathbf{w}}_{ij})_{|T} \ , \ 1 \le i, j \le 3 \, , \, i \ne j$$

with $\tilde{\mathbf{w}}_{ij}$ defined as in (15) over T.

Boundary triangles with one edge on Γ – We suppose that $\overline{T} \cap \partial\Gamma$ consists of one edge of T and that this edge is associated to the edge of $\hat{T}$ lying on $\hat{y} = 0$ (see Figure 4). The space $(M_h)_{|T}$ contains *four* functions $\varphi_k \in T_h$ with degrees of freedom defined in (16) for only the internal edges. The basis functions are

$$\varphi_{13} = (\tilde{\mathbf{w}}_{13})_{|T} \, , \quad \varphi_{31} = (\tilde{\mathbf{w}}_{31})_{|T} - (\tilde{\mathbf{w}}_{12})_{|\hat{T}} + (\tilde{\mathbf{w}}_{21})_{|T} \, ,$$
$$\varphi_{23} = (\tilde{\mathbf{w}}_{23})_{|T} \, , \quad \varphi_{32} = (\tilde{\mathbf{w}}_{32})_{|T} + (\tilde{\mathbf{w}}_{12})_{|\hat{T}} - (\tilde{\mathbf{w}}_{21})_{|T}$$

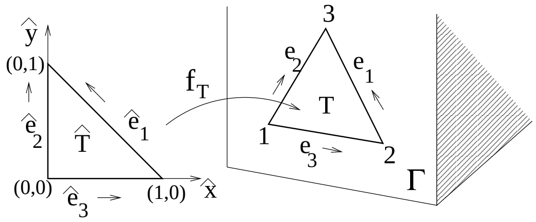

FIG. 3. *Orientation of the edges in the unit triangle $\hat{T}$ and on a current one T such that* $\overline{T} \cap \partial\Gamma = \emptyset$.

with $\tilde{\mathbf{w}}_{ij}$ defined as in (15) over T.

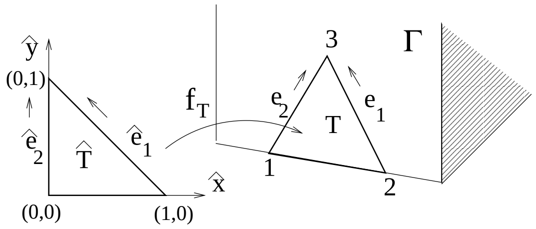

FIG. 4. *Orientation of the internal edges in the unit triangle $\hat{T}$ and in a current one T with one edge on* $\partial\Gamma$.

Boundary triangles with two edges on Γ – We suppose that $\overline{T} \cap \partial\Gamma$ consists of two edges of T and that these edges are associated to those of $\hat{T}$ lying on $\hat{y} = 0$ and $\hat{x} = 0$ (see Figure 5). The Lagrangian multipliers have to be built simultaneously on T and on the adjacent triangle T'. We denote by $\hat{T}'$ the rectangle triangle that complements $\hat{T}$ to a square. The triangle $\hat{T}'$ is obtained by applying to T' first the transformation that maps T' onto $\hat{T}$ (we choose the one that maps the common side between T and T' onto the hypothenuse of $\hat{T}$) and then a symmetry with respect to the line of equation $\hat{x} + \hat{y} = 1$ (we call $f_{T'}$ the transformation from $\hat{T}'$ to T'). The space $(M_h)_{|T \cup T'}$ contains *six* functions $\varphi_h \in T_h$ with tangential component continuous across the common edge. The degrees of freedom are those defined in (16) over the sides lying on $\hat{x} = 0$ and $\hat{y} = 0$ with $p \in I\!P_0$, for $\hat{T}$, and over the sides lying on $\hat{x} = 1$ and $\hat{y} = 1$ with $p \in I\!P_1$, for $\hat{T}'$. The basis functions are

$$
\begin{aligned}
\text{on } T' \quad & \varphi_{34} = (\tilde{\mathbf{w}}_{34})_{|T'} \quad , \quad \varphi_{43} = (\tilde{\mathbf{w}}_{43})_{|T'} \,, \\
& \varphi_{42} = (\tilde{\mathbf{w}}_{42})_{|T'} \quad , \quad \varphi_{24} = (\tilde{\mathbf{w}}_{24})_{|T'} \,, \\
\text{on } T \quad & \varphi_{13} = -(\tilde{\mathbf{w}}_{23})_{|T} + (\tilde{\mathbf{w}}_{32})_{|T} - (\tilde{\mathbf{w}}_{13})_{|T} + (\tilde{\mathbf{w}}_{31})_{|T} = (0,-1)^t \,, \\
& \varphi_{12} = (\tilde{\mathbf{w}}_{23})_{|T} - (\tilde{\mathbf{w}}_{32})_{|T} - (\tilde{\mathbf{w}}_{12})_{|T} + (\tilde{\mathbf{w}}_{21})_{|T} = (-1,0)^t
\end{aligned}
$$

with $\tilde{\mathbf{w}}_{ij}$ defined as in (15) over T and T'. Note that φ_{12} and φ_{13} are extended on T' by respectively $-(\tilde{\mathbf{w}}_{23})_{|T'} + (\tilde{\mathbf{w}}_{32})_{|T'}$ and $(\tilde{\mathbf{w}}_{23})_{|T'} - (\tilde{\mathbf{w}}_{32})_{|T'}$.

Rotations – Giving the expression of the Lagrange multipliers, we have made two hypotheses on T: first, that $T = \overline{K} \cap \Gamma$ is mapped through F_K on the face $\hat{T} = \hat{K} \cap \{\hat{z} = 0\}$ and, second, that if $\overline{T} \cap \partial\Gamma$ consists of one edge of T, this edge is mapped on the edge of $\hat{T}$ lying on $\hat{y} = 0$, and if $\overline{T} \cap \partial\Gamma$ consists of two edges of T, these edges are

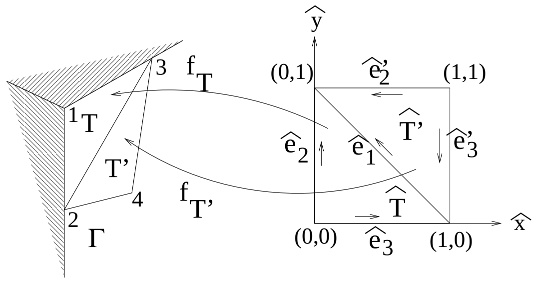

FIG. 5. *Transformation of $\hat{T} \cup \hat{T}'$ into $T \cup T'$ where T has two edges on $\partial\Gamma$.*

mapped on those of $\hat{T}$ lying on $\hat{y} = 0$ and $\hat{x} = 0$. In the general case, these hypotheses do not hold. It is then sufficient to rotate K, i.e. renumbering its nodes and edges, in such a way that the reference tetrahedron is in the "correct position" (see Figure 6 to catch the idea).

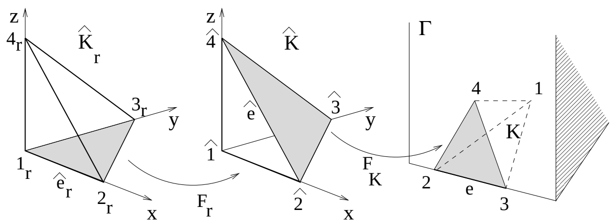

FIG. 6. *Sequence of transformations to pass from K to a unit tetrahedron in the "correct position". In this picture, we suppose that $\overline{K} \cap \Gamma = \overline{T} =$ face 2 3 4 of K and in addition $\overline{K} \cap \partial\Gamma =$ edge 2 3 of K. By using the transformation F_K^{-1} we have that the face 2 3 4 of K is transformed into the face $\hat{2}\,\hat{3}\,\hat{4}$ of $\hat{K}$ and the edge 2 3 of K is transformed into the edge $\hat{2}\,\hat{3}$ of $\hat{K}$. The additional transformation, named F_r^{-1}, transforms the face $\hat{2}\,\hat{3}\,\hat{4}$ of $\hat{K}$ into the face $1_r\,2_r\,3_r$ of $\hat{K}_r$ and the edge $\hat{2}\,\hat{3}$ of $\hat{K}$ into the edge $1_r\,2_r$ of $\hat{K}_r$ which is the "correct position" of the unit tetrahedron where we have computed the expression for the Lagrange multipliers. We thus replace F_K by $F_K \circ F_r$.*

2.3.2. Description of a basis for M_h in case the first family is used.

Internal triangles – We suppose that $\overline{T} \cap \partial\Gamma = \emptyset$ (see Figure 3) or reduced to one point. The space $(M_h)_T$ contains three functions $\varphi_h \in T_h$ with degrees of freedom defined in (14) for all the three edges. The basis functions are

$$\varphi_{ij} = (\mathbf{w}_{ij})_{|T} \ , \ 1 \leq i < j \leq 3 \,,$$

with $\mathbf{w}_{ij}$ defined as in (13) over T.

Boundary triangles with one edge on Γ – We suppose that $\overline{T} \cap \partial\Gamma$ consists of one edge of T and that this edge is associated to the edge of $\hat{T}$ lying on $\hat{y} = 0$ (see Figure 4). For such a triangle, imposing that one component is $\mathbb{P}_0$ implies here that both are $\mathbb{P}_0$. The space $(M_h)_T$ contains two functions $\varphi_h \in T_h$ with degrees of freedom defined in (14) for only the internal edges. The basis functions are

$$\varphi_{13} = (\mathbf{w}_{13})_{|T} + (\mathbf{w}_{12})_{|T} = (1,1)^t \quad , \quad \varphi_{23} = (\mathbf{w}_{23})_{|T} - (\mathbf{w}_{12})_{|T} = (-1,0)^t$$

with $\mathbf{w}_{ij}$ defined as in (13) over T.

Boundary triangles with two edges on Γ – We suppose that $\overline{T} \cap \partial\Gamma$ consists of two edges of T and that these edges are associated to those of $\hat{T}$ lying on $\hat{y} = 0$ and $\hat{x} = 0$ (see Figure 5). Here again, the adjacent triangle T' has to be involved. The degrees of freedom are those defined in (14) over the sides lying on $\hat{x} + \hat{y} = 1$, for $\hat{T}$, and over the sides lying on $\hat{x} = 1$ and $\hat{y} = 1$ for $\hat{T}'$. The basis functions are

$$\begin{aligned} &\text{on } T' \quad \varphi_{43} = (\mathbf{w}_{43})_{|T'} \quad , \quad \varphi_{42} = (\mathbf{w}_{42})_{|T'} \,, \\ &\text{on } T \quad\; \varphi_{23} = (\mathbf{w}_{23})_{|T}(x^M_{e_3}, y^M_{e_3}) = (\mathbf{w}_{23})_T - \tfrac{1}{2}(\mathbf{w}_{12})_T + \tfrac{1}{2}(\mathbf{w}_{13})_T \,, \end{aligned}$$

with $(x^M_{e_3}, y^M_{e_3})$ is the mid-point of e_3 and $\mathbf{w}_{ij}$ defined as in (13) over T and T'. Note that φ_{23} is extended on T' by $(\mathbf{w}_{23})_{|T'}$.

2.4. Merging the two families of edge elements. In the paper [3], the authors have shown that the mortar method combined with edge elements in three dimensions leads to an approximation which is slightly sub-optimal with the second family and give indications that with the first family non-optimal results could be feared (our results in Section 4 corroborate this fear). On the other hand, by using the second family of edge elements in one domain, the number of unknowns for a given mesh is multiplied by two even though, for a magnetostatic problem, both families lead to the same approximation accuracy for $\mathbf{u}_h$ and its curl (the expression curl $\mathbf{w}_{ij} = \text{grad}\ \lambda_i \wedge \text{grad}\ \lambda_j$ is valid with both families). The compromise to have a good approximation without too many unknowns is to limit (as proposed in [10]) the use of the second family to all edges that belong to the interface Γ. The first family is then adopted to approximate the problem solution along all edges that do not belong to the interface (i.e. over each tetrahedron that does not meet the interface). The idea is based on the following two facts:

- taking the difference of $\tilde{\mathbf{w}}_{ij}$ and $\tilde{\mathbf{w}}_{ji}$ defined in (15) we get the element $\mathbf{w}_{ij}$ defined in (13); moreover, one element $\mathbf{v} \in \mathcal{P}_1$ can be thought as an element $\mathbf{v} \in \mathcal{P}_2$ with the corresponding degrees of freedom $(\beta_{ij}, \beta_{ji}) = (\alpha_{ij}, -\alpha_{ij})$;
- the Lagrange multipliers of the mortar method are defined locally on Γ.

So, the space of edge elements $\mathcal{P}$ involved in (18) can be chosen as it follows:

$$\mathcal{P}(K) = \{\mathbf{u} \,|\, \mathbf{u}_{|e} \in \mathcal{P}_1 \,,\, \forall e \notin \partial K \cap \Gamma \ \text{ and } \mathbf{u}_{|e} \in \mathcal{P}_2 \,,\, \forall e \in \partial K \cap \Gamma \,\} \,. \tag{25}$$

In the following, we will refer to $\mathcal{P}$ as the *enriched family of edge elements.*

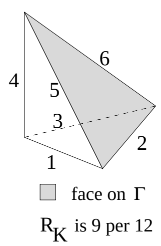

$$R^T_K = \begin{bmatrix} 1&0&0&0&0&0&0&0&0 \\ -1&0&0&0&0&0&0&0&0 \\ 0&1&0&0&0&0&0&0&0 \\ 0&0&1&0&0&0&0&0&0 \\ 0&0&0&1&0&0&0&0&0 \\ 0&0&0&-1&0&0&0&0&0 \\ 0&0&0&0&1&0&0&0&0 \\ 0&0&0&0&-1&0&0&0&0 \\ 0&0&0&0&0&1&0&0&0 \\ 0&0&0&0&0&0&1&0&0 \\ 0&0&0&0&0&0&0&1&0 \\ 0&0&0&0&0&0&0&0&1 \end{bmatrix}$$

FIG. 7. *The elements of matrix R^T_K for a given tetrahedron K; to each edge among those with numbers 1, 3, 4, is associated one circulation and to those with numbers 2, 5, 6, are associated two.*

From the implementation point of view, the merging can be done by introducing a rectangular matrix R_K that depends on the current tetrahedron K as follows:

$$\begin{array}{ll} R_K \in \mathcal{M}(6,12) & \partial K \cap \Gamma = \emptyset \text{ or reduced to one point} \\ R_K \in \mathcal{M}(7,12) & \partial K \cap \Gamma \text{ consists of one edge of } K\,, \\ R_K \in \mathcal{M}(9,12) & \partial K \cap \Gamma \text{ consists of one face of } K\,, \\ R_K \in \mathcal{M}(11,12) & \partial K \cap \Gamma \text{ consists of two faces of } K\,. \end{array}$$

Here, $\mathcal{M}(n,m)$ denotes the set of matrices with n rows and m columns. Moreover, the local stiffness matrix associated to each tetrahedron is built using the second family for only those elements K that meet the interface, i.e. $S_K \in \mathcal{M}(12,12)$ if $\partial K \cap \Gamma \neq \emptyset$ nor to one point. In this case, the assembling process does not involve the full matrix S_K but the smaller one given by $R_K S_K R_K^T$ (we have got rid of the additional unknowns for all edges of K that do not lie on Γ).

We end this Section by stating the convergence result concerning problem (5) with $\nu = 1$ (see [3] for a detailed proof).

THEOREM 2.1. *Let $\mathbf{u} \in H_0(\mathbf{curl}, \Omega)$ be the solution of problem (5) and $\mathbf{u}_h$ the solution of problem (24) with M_h defined by (21). We assume that $\mathbf{u}_k \in H^2(\Omega_k)$ with $\mathbf{curl}\,\mathbf{u}_k \in H^2(\Omega_k)$ $(1 \leq k \leq K)$ and we suppose that there exists a uniform constant γ such that $\max_k\{h_k\} \leq \gamma \min_k\{h_k\}$, $k = 1, 2$. We set $h := \max_k\{h_k\}$. The following estimate holds:*

$$||\mathbf{u} - \mathbf{u}_h||_{\star,\Omega} \leq C_1\, h \left(\sum_{k=1}^{K} ||\mathbf{u}||^2_{2,\Omega_k} \right)^{\frac{1}{2}} + C_2\, h \sqrt{|\ln h|} \left(\sum_{k=1}^{K} ||\mathbf{curl}\,\mathbf{u}||^2_{2,\Omega_k} \right)^{\frac{1}{2}}$$

where C_1, C_2 are uniform constants depending only on the macro-decomposition. Note that the first term comes from the best approximation error and the second one from the consistency error.

REMARK 2.2. *The same error estimate holds when the coefficients are not set equal to one but they jump through the different sub–domains: the constant in front of the right hand side will depend on the size of their jumps. The use of the first family inside each sub-domain together with the second one at the interface glued together with the mortar element method does not pollute the general accuracy of the method.*

3. Mortar condition discretization and problem matrix form. We now focus our attention on the numerical treatment of the constraint (23), involved in the definition of a basis for the space $\mathcal{U}_h^0$, and on the matrix form of problem (24). While the construction process does not depend on the choice of the edge elements we use (first family, second family or the merged family described above), this is not the case for the basis of $\mathcal{U}_h^0$. Here, we give the details in case the merged family is used.

3.1. A basis for the space $\mathcal{U}_h^0$. Two meshes $\mathcal{T}_{k,h_k}$ composed of tetrahedra with straight edges are used to discretize both domains and the associated discrete subspaces X_{k,h_k} are defined in (19). We denote by e_K the edges of K, and we define the sets Ξ_k, Ξ_k^0 as follows:

$$\Xi_k = \{e_K \,|\, K \in \mathcal{T}_{k,h_k}\} \quad , \quad \Xi_k^0 := \{e_K \,|\, K \in \mathcal{T}_{k,h_k},\, e_K \notin \partial\Omega_k \setminus \Gamma\}\,.$$

In defining the sets Ξ_h and Ξ_h^0, an assembly process has taken place and in the global numeration we will write the edges as e. In the following, we will say that one edge e

lays on Γ (and we will note this by writing $e \in \Gamma$) if it belongs to a triangle of $(\mathcal{T}_{k,h_k})_{|\Gamma}$ (k= 1,2). The edges lying on the interface will be divided into three sets, that are:

$$\xi^k = \{e \in \Xi_k \cap \Gamma\} \quad , \quad \xi_0^k = \{e \in \Xi_k^0 \cap \Gamma\} \quad , \quad \xi_{\partial\Gamma}^k = \xi^k \setminus \xi_0^k \,.$$

We denote by m_Γ^k, $m_{\partial\Gamma}^k$, $m_{\Gamma\setminus\partial\Gamma}^k$ and m^k the number of degrees of freedom associated to all edges belonging to ξ^k, $\xi_{\partial\Gamma}^k$, ξ_0^k and Ξ_k, respectively. We note that $m_{\Gamma\setminus\partial\Gamma}^k = m_\Gamma^k - m_{\partial\Gamma}^k$.

To shorten the notation, let us denote by $\mathbf{w}^1$, $\tilde{\mathbf{w}}^1$ the basis functions associated to edges of Ξ_1 of, respectively, the first and second family, and by $\mathbf{w}^2$, $\tilde{\mathbf{w}}^2$ the basis function associated to edges of Ξ_2 of, respectively, the first and second family. These functions are the elements of the spaces Y_{k,h_k} (k=1,2) of the forms (13) or (15). Let us denote by $\mathcal{B}$ a basis for $\mathcal{U}_h^0$: we suppose that $\mathcal{B} = \mathcal{B}^1 \cup \mathcal{B}^2 \cup \mathcal{B}^{\Gamma_1} \cup \mathcal{B}^{\Gamma_2}$ where the sets of functions $\mathcal{B}^1$, $\mathcal{B}^2$, $\mathcal{B}^{\Gamma_1}$ and $\mathcal{B}^{\Gamma_2}$ will be defined below.

The functions in $\mathcal{B}^1$ are zero in $\overline{\Omega^2}$, the functions in $\mathcal{B}^2$ are zero in $\overline{\Omega^1}$, and the functions in $\mathcal{B}^{\Gamma_1} \cup \mathcal{B}^{\Gamma_2}$ have their support in the union of the *mortar* elements, i.e. tetrahedra with at least one face on Γ. Due to the properties of the considered basis functions, we set:

$$\mathcal{B}^1 = \{(\mathbf{w}_s^1, \mathbf{0}) \,|\, s \,:\, e_s \in \Xi_1 \setminus \xi^1\} \quad , \quad \mathcal{B}^2 = \{(\mathbf{0}, \mathbf{w}_r^2) \,|\, r \,:\, e_r \in \Xi_2 \setminus \xi^2\} \,; \tag{26}$$

a possible choice for the basis functions associated on edges lying on the interface is

$$\begin{aligned} \mathcal{B}^{\Gamma_1} &= \Big\{ (\tilde{\mathbf{w}}_s^1 \,,\, \textstyle\sum_{r\,:\,e_r \in \xi_0^2} q_r^s \tilde{\mathbf{w}}_r^2) && |\, q_r^s \in I\!\!R \text{ and } s \,:\, e_s \in \xi^1 \Big\} \,, \\ \mathcal{B}^{\Gamma_2} &= \Big\{ (\mathbf{0} \,,\, \tilde{\mathbf{w}}_s^2 + \textstyle\sum_{r\,:\,e_r \in \xi_0^2} q_r^s \tilde{\mathbf{w}}_r^2) && |\, q_r^s \in I\!\!R \text{ and } s \,:\, e_s \in \xi_{\partial\Gamma}^2 \Big\} \,. \end{aligned} \tag{27}$$

For each of the $m_\Gamma^1 + m_{\partial\Gamma}^2$ indices s, the coefficients q_r^s, $r = 1, m_{\Gamma\setminus\partial\Gamma}^2$, are determined by imposing, the integral matching condition (note that dim $(M_h) = m_{\Gamma\setminus\partial\Gamma}^2$)

$$\int_\Gamma [\, (\tilde{\mathbf{w}}_s)_{T,\Gamma} - \sum_{r: e_r \in \xi_0^2} q_r^s (\tilde{\mathbf{w}}_r^2)_{T,\Gamma} \,] \cdot \varphi_k \, d\Gamma = 0 \qquad \forall\, \varphi_k \in M_h \tag{28}$$

where $\tilde{\mathbf{w}}_s = \tilde{\mathbf{w}}_s^1$ for all indices s such that $e_s \in \xi_\Gamma^1$ and $\tilde{\mathbf{w}}_s = -\tilde{\mathbf{w}}_s^2$ for all indices s such that $e_s \in \xi_{\partial\Gamma}^2$. Each of these $m_\Gamma^1 + m_{\partial\Gamma}^2$ sets of $m_{\Gamma\setminus\partial\Gamma}^2$ equations can be put into the following matricial form $C\mathbf{q}^s = D(\cdot, s)$ where

$$C(k,r) = \int_\Gamma (\tilde{\mathbf{w}}_r^2)_{T,\Gamma} \cdot \varphi_k \, d\Gamma \qquad\qquad r \,:\, e_r \in \xi_0^2 \quad , \, k : \varphi_k \in M_h, \tag{29}$$

$$D(k,s) = \int_\Gamma (\tilde{\mathbf{w}}_s)_{T,\Gamma} \cdot \varphi_k \, d\Gamma \qquad \begin{array}{ll} \tilde{\mathbf{w}}_s = \tilde{\mathbf{w}}_s^1 & s \,:\, e_s \in \xi^1 \\ \tilde{\mathbf{w}}_s = -\tilde{\mathbf{w}}_s^2 & s \,:\, e_s \in \xi_{\partial\Gamma}^2 \end{array} \quad , \, k : \varphi_k \in M_h \,. \tag{30}$$

The system (28) allows us to determine the vector $\mathbf{q}^s$ for all edges $e_s \in \xi^1 \cup \xi_{\partial\Gamma}^2$ and thus the set of basis functions on the interface. For the matrix form of problem (24), it is usefull to define the rectangular matrix Q of dimension $m_{\Gamma\setminus\partial\Gamma}^2 \times (m_\Gamma^1 + m_{\partial\Gamma}^2)$

$$Q = C^{-1} D = [Q_1, Q_2]$$

with Q_1 of dimension $m_{\Gamma\setminus\partial\Gamma}^2 \times m_\Gamma^1$ and Q_2 of dimension $m_{\Gamma\setminus\partial\Gamma}^2 \times m_{\partial\Gamma}^2$. The matrix Q allows to couple at the interface the information coming from the Ω_1 and Ω_2 domains and its construction is a crucial point in the implementation of the method. In presence of movement, Q has to be rebuilt at each new configuration of the free part. In the following, we explain an easy procedure to numerically compute the involved integrals over Γ.

3.2. Numerical treatment of the coupling condition. In two dimensions we could intersect the two different discretizations of Γ since the involved geometric entities were segments. In three dimensions, the intersection between two triangles (that can even live on non-complanar surfaces, as it happens with curved interfaces) becomes a hard task. To overcome the problem and compute the integrals in (30) we have to act differently by introducing for the interface only a *third mesh*, named $\mathcal{T}^{\Gamma}_{3,h_3}$, over Γ, i.e. a discretization of Γ independent of the ones given by $(\mathcal{T}_{k,h_k})_{|\Gamma}$ (k = 1,2) (see Figure 8).

It is natural to ask why we do not use one of the two existing surface discretizations $(\mathcal{T}_{k,h_k})_{|\Gamma}$ (k = 1,2) for the numerical integration of the coupling condition. The choice of introducing a third mesh is due to several reasons. Among them, we do not want to "favour" one discretization with respect to the other. Secondly, taking one of the two interface meshes leads to a lack of accuracy as explained in [11]. In addition, we can refine the integration mesh $\mathcal{T}^{\Gamma}_{3,h_3}$ independently of the existing two, in order to get a better accuracy in computing the surface integrals.

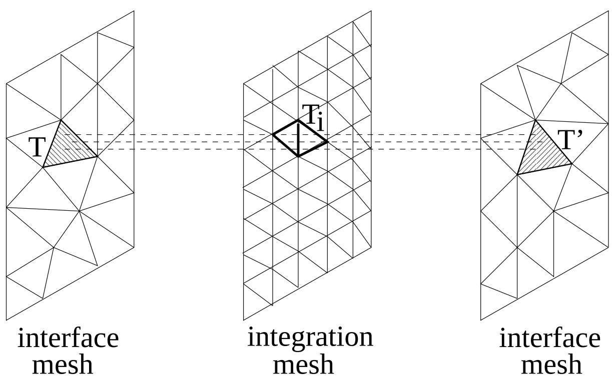

FIG. 8. *Projection of the quadrature nodes defined on the triangles of $\mathcal{T}^{\Gamma}_{3,h_3}$ on $(\mathcal{T}_{k,h_k})_{|\Gamma}$ (k = 1,2). The quadrature nodes contained in the triangles put in evidence on the integration mesh are used to compute the surface integrals (30) over $T \cap T'$ with $T \in (\mathcal{T}_{1,h_1})_{|\Gamma}$ and $T' \in (\mathcal{T}_{2,h_2})_{|\Gamma}$.*

The computation of the integral $\int_\Gamma (\tilde{\mathbf{w}}^1_s)_{T,\Gamma} \cdot \varphi_k \, d\Gamma$ can be done through the following steps:
(i) we define a quadrature formula $(\omega^j_i, \mathbf{x}^j_i)$ $(j = 1, N_q)$ on the mesh triangles T_i of $\mathcal{T}^{\Gamma}_{3,h_3}$ by transforming a chosen quadrature formula defined on the unit triangle $\hat{T}$;
(ii) we build a radial projection operator from triangles of $\mathcal{T}^{\Gamma}_{3,h_3}$ to triangles of $(\mathcal{T}_{k,h_k})_{|\Gamma}$;
(iii) we project each node $\mathbf{x}^j_i$ on $(\mathcal{T}_{1,h_1})_{|\Gamma}$ and we call $\mathbf{x}^j_{i,1}$ the projected node;
(iv) we project each node $\mathbf{x}^j_i$ on $(\mathcal{T}_{2,h_2})_{|\Gamma}$ and we call $\mathbf{x}^j_{i,2}$ the projected node.
We then have

$$\int_\Gamma (\tilde{\mathbf{w}}^1_s)_{T,\Gamma} \cdot \varphi_k \, d\Gamma = \sum_{T_i \in \mathcal{T}^{\Gamma}_{3,h_3}} \sum_{j=1}^{N_q} \omega^j_i \, (\tilde{\mathbf{w}}^1_s)_{T,\Gamma}(\mathbf{x}^j_{i,1}) \cdot \varphi_k(\mathbf{x}^j_{i,2}) \, .$$

The results we present in Section 4 have been obtained by using quite a fine grid $\mathcal{T}^{\Gamma}_{3,h_3}$ on the interface Γ with $N_q = 2$. The sensibility of the numerical results to the choice of this third mesh has not been analysed yet: in this paper we have focused the attention on the method precision assuming that the integrals on Γ are computed in an "almost" analytical way.

3.3. Matrix form of the discretized problem. The system we solve to get numerical results is built exactly as explained in [9, 23]. So, we start by writing, in each sub-domain, the final system associated to equation (24) with homogeneous Neumann type conditions on the interface Γ. Then the two systems are coupled by means of the mortar condition.

Let $(\mathbf{u}_{1,h}, \mathbf{u}_{2,h})$ be the solution of the fully discrete problem: we expand it in terms of the edge element basis functions of the finite dimensional spaces X_{k,h_k} (k=1,2) defined in the sub-domains. We then have m^1 unknown coefficients u^1_s and m^2 unknown coefficients u^2_r. If we choose Ω_1 as master sub-domain for the unknown values associated to the edges lying on the interface, among the $m^1 + m^2$ coefficients, only $m^1 + m^2 - m^2_{\Gamma\setminus\partial\Gamma}$ are real unknowns. In fact, the $m^2_{\Gamma\setminus\partial\Gamma}$ coefficients associated to edges in ξ^2_0 are linked to the $m^1_\Gamma + m^2_{\partial\Gamma}$ coefficients associated to those in $\xi^1_\Gamma \cup \xi^2_{\partial\Gamma}$ through the mortar condition.

We divide the unknowns in each sub-domain in three blocks with names reported in parentheses: the first block $(\mathbf{u}^k_{\partial\Gamma})$ contains the unknowns associated to edges in $\xi^k_{\partial\Gamma}$, the second block $(\mathbf{u}^k_{\Gamma\setminus\partial\Gamma})$ contains the unknowns associated to edges in $\xi^k_{\Gamma\setminus\partial\Gamma}$ and the third block $(\mathbf{u}^k_{Int})$ those associated to edges in $\Xi^k \setminus \xi^k$ $(k = 1, 2)$.

In each sub-domain, we build the system associated to the fully discrete problem equations with a homogeneous Neumann condition at the interface Γ. In this way, we obtain two linear systems of the following form $(k = 1, 2)$

$$S^k \begin{pmatrix} \mathbf{u}^k_{\partial\Gamma} \\ \\ \mathbf{u}^k_{\Gamma\setminus\partial\Gamma} \\ \\ \mathbf{u}^k_{Int} \end{pmatrix} = \begin{pmatrix} \mathbf{F}^k_{\partial\Gamma} \\ \\ \mathbf{F}^k_{\Gamma\setminus\partial\Gamma} \\ \\ \mathbf{F}^k_{Int} \end{pmatrix}.$$

where $(\mathbf{F}^k_{\partial\Gamma}, \mathbf{F}^k_{\Gamma\setminus\partial\Gamma}, \mathbf{F}^k_{Int})$ is the vector associated to the right-hand side of problem (24) in Ω_k and S^k is the standard stiffness built by assembling, $\forall K \in \mathcal{T}_{k,h_k}$, the local matrices S_K or $R_K S_K R^t_K$ depending whether $\dim(\partial K \cap \Gamma) = 0$ or not.

Neither $\mathbf{u}^1$ nor $\mathbf{u}^2$ are solutions of the previous problems since the two sets of values $((\mathbf{u}^1_{\partial\Gamma}, \mathbf{u}^1_{\Gamma\setminus\partial\Gamma}), \mathbf{u}^2_{\partial\Gamma})$ and $\mathbf{u}^2_{\Gamma\setminus\partial\Gamma}$ are linked one to the other by the mortar matching condition. Choosing Ω_1 as master sub-domain, we have

$$\mathbf{u}^2_{\Gamma\setminus\partial\Gamma} \;=\; [Q_1, Q_2]\,((\mathbf{u}^1_{\partial\Gamma}, \mathbf{u}^1_{\Gamma\setminus\partial\Gamma}), \mathbf{u}^2_{\partial\Gamma})^t$$

where $Q = [Q_1, Q_2]$ is the rectangular full matrix of dimension $m^2_{\Gamma\setminus\partial\Gamma}$ per $m^1_\Gamma + m^2_{\partial\Gamma}$ obtained from the matching condition discretization. We introduce then the following matrices:

$$\tilde{Q} = \begin{pmatrix} Id & 0 & 0 & 0 \\ 0 & Id & 0 & 0 \\ 0 & 0 & Id & 0 \\ Q_1 & 0 & Q_2 & 0 \\ 0 & 0 & 0 & Id \end{pmatrix} \quad \text{and} \quad S = \begin{pmatrix} S^1 & 0 \\ 0 & S^2 \end{pmatrix} \tag{31}$$

Indicating by $\mathbf{y}$ the independent unkowns, i.e. $\mathbf{y} = \left((\mathbf{u}^1_{\partial\Gamma}, \mathbf{u}^1_{\Gamma\setminus\partial\Gamma}), \mathbf{u}^1_{Int}, \mathbf{u}^2_{\partial\Gamma}, \mathbf{u}^2_{Int} \right)^t$, the approximation of the physical solution is computed solving the system

$$\tilde{Q}^t \; S \; \tilde{Q}\mathbf{y} \;=\; \tilde{Q}^t\mathbf{F} \tag{32}$$

The final system is solved by an iterative, Jacobi preconditioned, Conjugate Gradient procedure. We remark that, thanks to the mortar method philosophy, residuals can be computed in parallel as observed in [4]. In particular, if we do not want to deal with the assembled matrix $\tilde{Q}^t S \tilde{Q}$, we have to work with the "objects" $\tilde{Q}$, S^k $(k = 1, 2)$ separately. For a vector $\mathbf{v} \in I\!R^n$ with $n = m^1 + m^2 - m^2_{\Gamma\setminus\partial\Gamma}$, the matrix-vector product $\tilde{Q}^t S \tilde{Q}\mathbf{v}$ can be done in three sequential steps:
$(step_1)$ we compute $\mathbf{q} = \tilde{Q}\mathbf{v}$ with $\mathbf{q} \in I\!R^s$ with $s = m^1 + m^2$;
$(step_2)$ we compute $\mathbf{p} = S\mathbf{q}$ separately in each sub-domain, i.e. $\mathbf{p}^k = S^k\mathbf{q}^k$ for $k = 1, 2$;
$(step_3)$ we compute $\mathbf{w} = \tilde{Q}^t\mathbf{p}$ with $\mathbf{w} \in I\!R^n$.
In this three-step product, the most expensive step is the second one due to the size of the sub-domain matrices; the products involving the coupling matrix are not expensive at all (the number of edges, and consequently of the unknowns, on Γ is inferior to that in the adjacent volume and the Lagrange multiplier supports on Γ are small). The Jacobi preconditioned CG algorithm that we have used is classical but the matrix-vector products have been done as explained. As a consequence, the inversion of (32) is accomplished with a sensible gain in time and without involving additional memory space.

4. Numerical results. In this section we are going to present some numerical results to show how the mortar element method coupled with the enriched first family of edge elements works. The problem on which the method has been tested is the calculation of the magnetic induction $\mathbf{B}$ given by a uniform current in a cube of uniform permeability corresponding to the homogeneous boundary condition $\mathbf{B}\cdot\mathbf{n} = 0$ on $\partial\Omega$. The magnetic permeability is that of the vacuum.

We consider the domain presented in Figure 1 where $\Omega = \Omega_1 \cup \Omega_2 \cup \Gamma$ is a cube of side $L = 1$ m. The mortar interface is the flat surface $\Gamma = \{(0.5, y, z) \mid 0 \le y \le 1, 0 \le z \le 1\}$. The chosen data give rise to a magnetic vector potential which is tangent to the interface: the mortar method is then used to couple a non-negligeable information.

In Table 1, we report, per sub-domain, the mesh data and the number of degrees of freedom (we indicate in parenthesis the number of degrees of freedom on the interface Γ). The matrices are stored in symmetric morse format, i.e. only their non-zero entries are considered. The non-conformity of the discretization at the common interface Γ is here achieved in two ways: 1) either we choose the same mesh in both sub-domains and we rotate of 90° one mesh with respect to the other; 2) or we consider a fine mesh in one sub-domain and a coarse mesh in the other sub-domain.

TABLE 1
Mesh data and degrees of freedom per sub-domain (on the interface)

meshes	nodes	elements	edges	degrees of freedom
I	27	48	98	42 (16)
II	59	166	272	168 (40)
III	125	384	604	396 (80)
IV	320	1294	1799	1411 (170)
V	343	1296	1854	1398 (192)
VI	729	3072	4184	3384 (352)
VII	1331	6000	7930	6690 (560)

In all simulations, the third mesh $\mathcal{T}^{\Gamma}_{3,h_3}$, introduced to numerically compute the integrals appearing in the coupling condition, is composed of 620 triangles and 345 nodes. For each of its triangles, we consider three internal integration nodes ($N_q =$ 3) corresponding in $\hat{T}$ to the points of coordinates $(\frac{1}{6}, \frac{1}{6})$, $(\frac{2}{3}, \frac{1}{6})$ and $(\frac{1}{6}, \frac{2}{3})$. The quadrature formula weights are equal to $\frac{1}{3}$. This quadrature formula has order two. On the third mesh we simulate, in some sense, an "exact" integration of all integrals over Γ even if the exact integration is in general never expected even by using a higher order quadrature formula: the coupling condition concerns indeed piecewise polynomials of degree two that are locally regular on almost all the triangles of the third fine mesh.

By the way, the third mesh has not to be too coarse since we risk to have a couple of triangles on Γ from Ω_1 and Ω_2 which does not interact since none of the integration nodes fall simultaneously in the two triangles.

In the following tables, we report the real number of degrees of freedom for various discretizations together with the final residual and number of iterations of the used Conjugue Gradient procedure. The tables also display the values of the stored magnetic energy obtained for a uniform density current of intensity 10^7 A/m^2 directed along the y-axis. In all examples, the vector $\mathbf{T}$ such that $\mathbf{curl}\,\mathbf{T} = \mathbf{J}$ is $\mathbf{T} = (0, 0, \mathrm{T}_0(x - .5))$ with $\mathrm{T}_0 = 10^7$ A/m. The computed value W_h for the stored magnetic energy has to be compared with the analytical one given by (see [1])

$$W_a = \frac{\mathrm{J}^2 L^5}{\nu_0} \left(\frac{1}{24} + \frac{8}{\pi^5} \sum_{n=0}^{\infty} \frac{\tanh(2\pi + 1)\pi/2}{(2n + 1)^5} \right).$$

For the considered situation, the analytical value of the energy is 2.208 MJ and the magnetic induction $\mathbf{B}$ has a maximum intensity of 3.9 Wb/m^2. It can be seen that the energy values obtained by the magnetic vector potential formulation are always approximated from below and the finer the mesh is, the closer the computed energy value is to the analitical one.

In Table 2, results address to the conforming case where both sub-domains are discretized with the same mesh. In this case, the coupling matrix Q is squared and "equivalent" to the identity. For each row i of Q, there exists only one column j such that $Q(i,j) \neq 0$ and $Q(i,j) = 1$, with j not necessarily equal to i due to the different numerotation of the degrees of fredoom in each sub-domain.

In Tables 3, results address to the non-conforming case where both sub-domains are discretized either with the same mesh (the second rotated of 90° with respect to the first one) or with different meshes. In this case, the coupling matrix Q is rectangular

TABLE 2
Conforming discretizations and enriched family of edge elements

meshes	dof	CG residual/ 10^{-7}	CG iterations	energy/10^6
I - I (*)	68	4.7063	20	1.5419
II - II	296	9.7081	30	1.9261
III - III (*)	712	9.9794	43	2.0271
IV - IV	2652	9.9279	52	2.1267
V - V	2604	8.9139	67	2.1267
VI - VI	6416	9.4174	90	2.1622
VII - VII	12820	9.4468	113	2.1787

and no more "equivalent" to the identity. The use of meshes that do not match at the interface does not spoil the numerical results. Note in fact that the magnetic energy value in Table 3 corresponding to a computation lead on the mesh configuration I - III is "in between" the values in Table 2 corresponding to computations lead on similar mesh configurations (I - I and III - III). Similarly for the magnetic energy value in Table 3 corresponding to a computation lead on the mesh configuration II - IV with respect to the values in Table 2 corresponding to computations lead on the mesh configurations II - II and IV - IV.

TABLE 3
Non-conforming discretizations and enriched family of edge elements

meshes	dof	CG residual/10^{-7}	CG iterations	energy/10^6
I - I rotated	68	7.3256	53	1.5521
III - I	358	7.8839	35	1.7466
I - III	422	9.2364	141	1.7764
I - III rotated	422	9.6712	127	1.7779
II - II rotated	296	9.7265	75	1.9195
II - IV	1539	9.7055	143	2.0216
II - IV rotated	1539	9.6157	142	2.0264
III - III rotated	712	9.7021	92	2.0277
IV - IV rotated	2652	9.6514	108	2.1318
V - V rotated	2604	9.9828	116	2.1267
VI - VI rotated	6416	9.9618	135	2.1621
VI - VII (*)	9722	9.8627	193	2.1703
VII - VI (*)	9514	9.7641	186	2.1703
VII - VII rotated	12820	9.7970	194	2.1786

In Figures 9 and 10 we present the magnetic induction distribution in the section of equation $y = 0.25$ computed on non-matching meshes VII - VI and VI - VII respectively. Colors refer to the vector intensity (in $\mathrm{Wb/m^2}$) and arrows are the renstrictions to the plane $y = 0.25$ of the magnetic induction vectors associated to the element barycenters. The corresponding energy values are indicated in the rows denoted by (*) of Table 3. Looking at the pictures, we see that the information is correctly transferred from the master to the slave sub-domain despite the discretizations do not match at the interface and even when the master mesh is coarser than the slave one. Moreover, the maximum of the computed magnetic induction intensity (on the top of the color scale reported on the right of the pictures) is equal to the

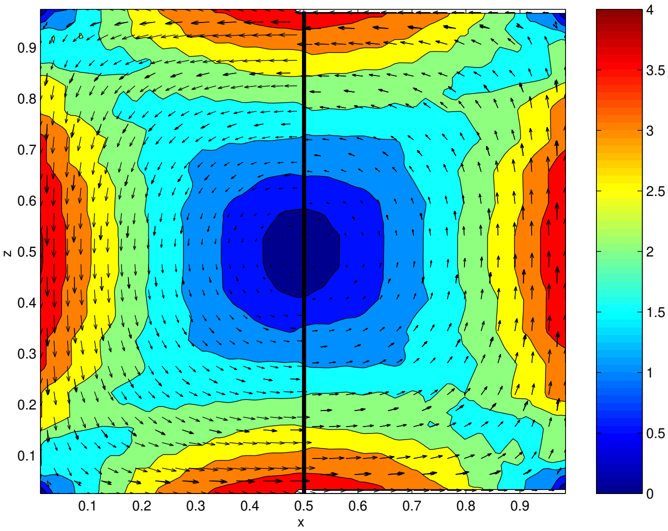

FIG. 9. *Magnetic induction on the section $y = 0.25$ of $[0,1]^3$: colors refer to the induction intensity (in Wb/m^2) and arrows refer to the renstriction to the section of the induction vector computed at the tetrahedra barycenters. The dark line separates the two sub-domains. Here, the master mesh is finer ($h_1 < h_2$).*

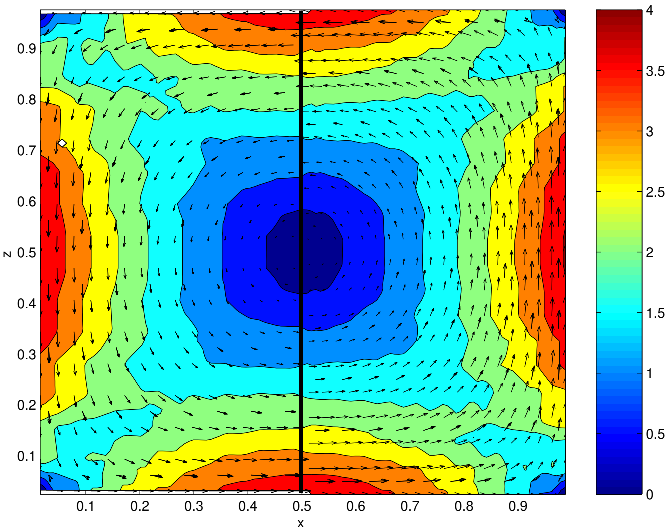

FIG. 10. *Magnetic induction on the section $y = 0.25$ of $[0,1]^3$: colors refer to the induction intensity (in Wb/m^2) and arrows refer to the renstriction to the section of the induction vector computed at the tetrahedra barycenters. The dark line separates the two sub-domains. Here, the master mesh is coarser ($h_1 > h_2$).*

analytical one. We remark that the theoretical analysis predicts the same optimal estimate for the approximation error in both cases when the slave mesh is corser or finer than the master one. This is confirmed by the numerical results: the magnetic energy is 2.1703 MJ in both cases. On the other hand, the number of iterations is meaningless since the solving procedure is not optimal at all.

By looking at Figures 9 and 10, it has to be remembered that the computed vector is the magnetic vector potential $\mathbf{u}_h$ whereas the displayed vector is the magnetic induction $\mathbf{B}_h$. The representation of the computed magnetic induction $\mathbf{B}_h$ on a plane $y =$ constant allows to better put in evidence the continuity across the mortar interface of the normal component of $\mathbf{B}_h$, despite the non-conformity of the sub-domain discretizations at that interface. In order to underline the continuity across the interface Γ of the tangential component of the computed magnetic vector potential, a representation of $\mathbf{u}_h$ on the plane $x = 0.5$ has to be considered: this representation is possible but more difficult to "read" since it involves two sets of arrows lying on the same plane.

We now investigate the precision of the proposed method by considering the dependence of the relative error $(W_a - W_h)/W_a$ for the stored magnetic energy on the mesh parameter h (i.e. the maximum diameter of the tetrahedra contained in the meshes discretizing the sub-domains).

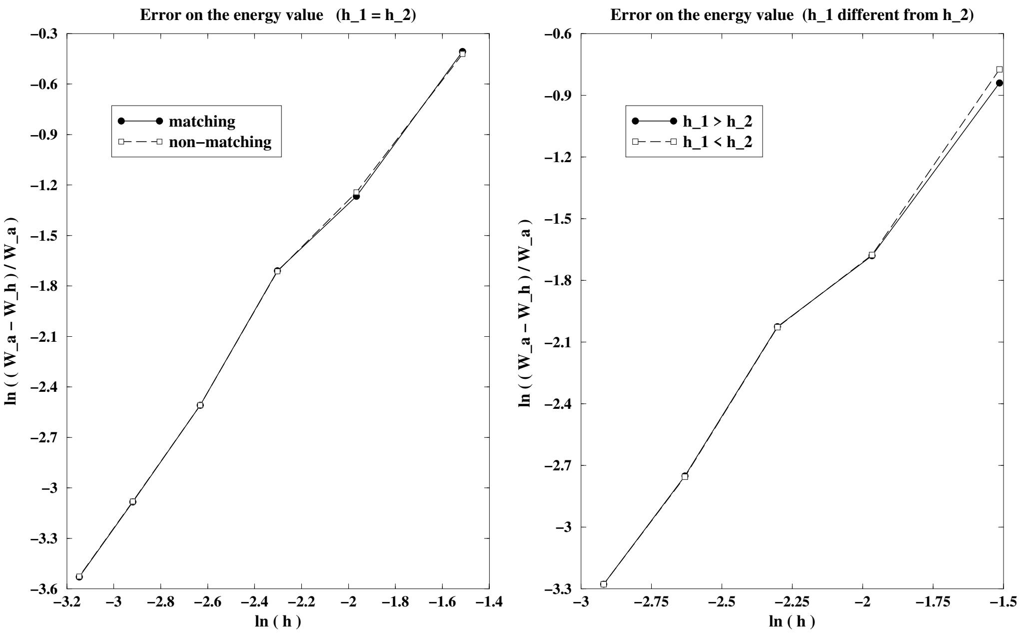

FIG. 11. *Relative error (in logarithm scale) on the stored magnetic energy. On the left, both sub-domains are discretized by the same mesh ($h_1 = h_2$): the triangular discretizations, induced on the interface by the sub-domain meshes, are either conforming or (when one mesh is rotated with respect to the other) non-conforming. On the right, the two sub-domains are discretized with different meshes ($h_1 \neq h_2$): the triangular discretizations induced on the interface by the sub-domain meshes are non-conforming.*

In Figure 11(left), the relative error is computed in the case where both sub-domains are discretized by the same mesh. Whether the two triangular discretizations of Γ, induced by the sub-domain meshes, match or not, the error is the same and decreases linearly with the mesh parameter h, as predicted by the theoretical analysis.

In Figure 11(right), we analyse the influence of the master mesh element size h_1 on the precision of the method. The relative error is then computed twice, taking the master mesh finer ($h_1 < h_2$) or coarser ($h_1 > h_2$) than the slave one. We can observe that the error is the same in both cases and decreases linearly with h_1. A similar figure can be obtained by displaying the dependence of the relative error on h_2.

In Table 4, results are about the non-conforming case where both sub-domains are discretized with the same mesh (the second rotated of 90° with respect to the first one): results are obtained by approximating the solution on the interface by using either the first or the second family of edge elements.

TABLE 4
Different edge element families on the interface

meshes	family	dof	CG res./10^{-7}	CG iter.	energy/10^6
III - III rotated	first	672	8.9823	58	1.8921
III - III rotated	enriched	712	9.7021	92	2.0277
IV - IV rotated	first	2567	9.5748	227	2.0916
IV - IV rotated	enriched	2652	9.6514	108	2.1318

In [3], authors have proven optimal error estimates when the second family of edge elements is used to approximate the solution on the interface Γ. Concerning the use of the first family of edge elements on Γ, numerical results confirm the feared non-optimality of the approximation: we have in fact that with the second family, the computed value for the magnetic energy is closer to the analytical one. We thus underline the importance of using the second family of edge elements on the common interface for a more accurate transfer of the information from one sub-domain to the other.

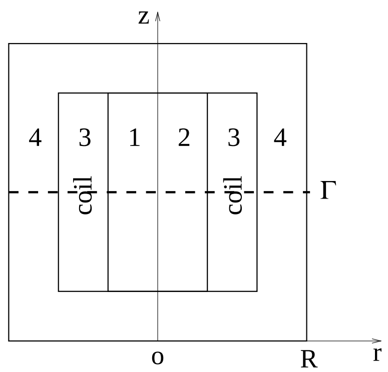

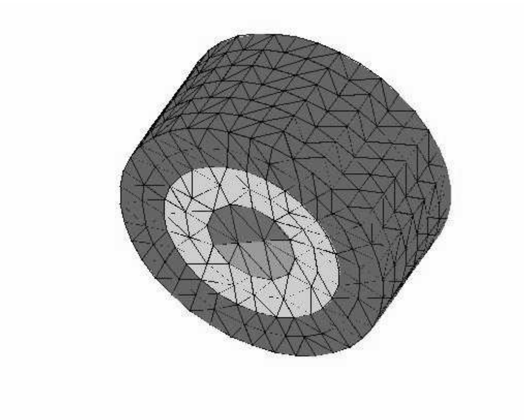

FIG. 12. *On the left, domain geometry on the section $\theta = 0$ orthogonal to the cylinder basis: four regions with magnetic reluctivity $\nu_1 = \nu_3 = \nu_0$ and $\nu_2 = \nu_4 = 0.1\ \nu_0$ respectively. Region (3) is a coil of height $h = 0.04$ m, internal radius $r_1 = 0.01$ m, external radius $r_1 = 0.02$ m, feeded with a constant density current $\mathbf{J} = 12.5\,10^4\ A/m^2$. The dashed line Γ denotes the position, on the considered section, of the interface between the lower Ω_1 and upper Ω_2 parts. On the right, the tetrahedrical mesh used to discretize the upper part (one color for each of the four regions).*

What follows is another example of application of the method. Let us consider a bounded cylinder with axis equal to the z-axis, height $H = 0.06$ m and radius $R = 0.03$ m. This cylinder is splitted into four nested regions filled with materials of different magnetic reluctivities (see Figure 12(left)): an exterior layer (4), a coil (3), an interior cylinder divided again in two regions (1) and (2). The domain is then cut in two parts (lower part Ω_1 and upper part Ω_2) by the flat interface $\Gamma = \{(r, \theta, z) \mid 0 \leq r \leq$

$R\,,\ 0 \le \theta \le 2\,\pi\,,\ z = 0.03\}$ (denoted by the dashed line on Figure 12(left)). We aim at computing the magnetic induction $\mathbf{B}$ given by the current in the coil corresponding to homogeneous boundary conditions $\mathbf{B}\cdot\mathbf{n} = 0$ on $\partial\Omega$ for different positions of the lower part. Being allowed to use non-matching grids at Γ, all the computation can be run on the initial mesh where the lower part has been suitably rotated. When the coil is circular with axis equal to the z-axis and the density current $\mathbf{J}$ is constant, as in this case, we have the analytical form $\mathbf{T} = (Ar + B)\mathbf{e}_z$ with

$$A = \frac{T_1 - T_2}{r_1 - r_2} \qquad \text{and} \qquad B = \frac{r_1 T_2 - r_2 T_1}{r_1 - r_2}$$

being r_i (i=1,2) the external and internal radii of the coil and $T_1 = 0$, $T_2 = 12.5\,10^2$ A/m the intensity values of $\mathbf{T}$ on the boundary surfaces of radius r_i (i = 1,2).

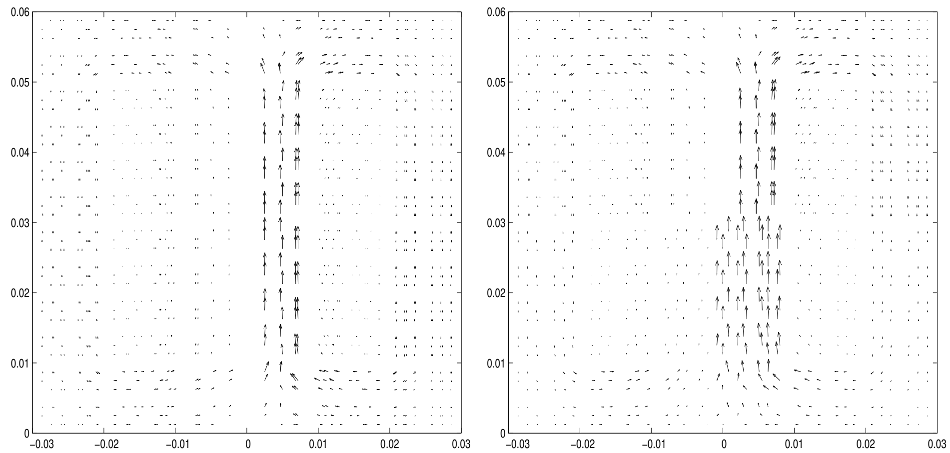

FIG. 13. *Magnetic induction distribution in the section $\theta = 0$ orthogonal to the cylinder basis: on the left, the lower part is in its original position whereas, on the right, it has rotated of 90° around the cylinder axis.*

In Figures 13 and 14, we present the magnetic induction distribution in the section $\theta = 0$ orthogonal to the cylinder basis for four different positions of the lower part. Arrows indicate the restriction to the considered section of the magnetic induction vector computed at the tetrahedra' barycentres. By looking at the pictures, we can see as the field distribution changes according to the lower part position in order to follow the way of minimum magnetic reluctivity, as it happens in a switched reluctance engine.

5. Conclusions. A non-conforming approximation of the three-dimensional magnetostatic problem has been presented and analysed mainly from the implementation point of view. Based on the mortar edge element method, this approximation has allowed to work in a very elegant way with domain discretizations that do not match at the interface. The interest of the proposed method is focused on the following issues: (1) the imposition at a discrete level of the transmission condition for the tangential component of the magnetic vector potential field across the interface, is done without any contraint between the spatial discretization steps h_1 and h_2; (2) the use of second order edge elements on the interface is mandatory to have an optimal approximation of the problem solution; (3) non-matching grids can be easily intersected

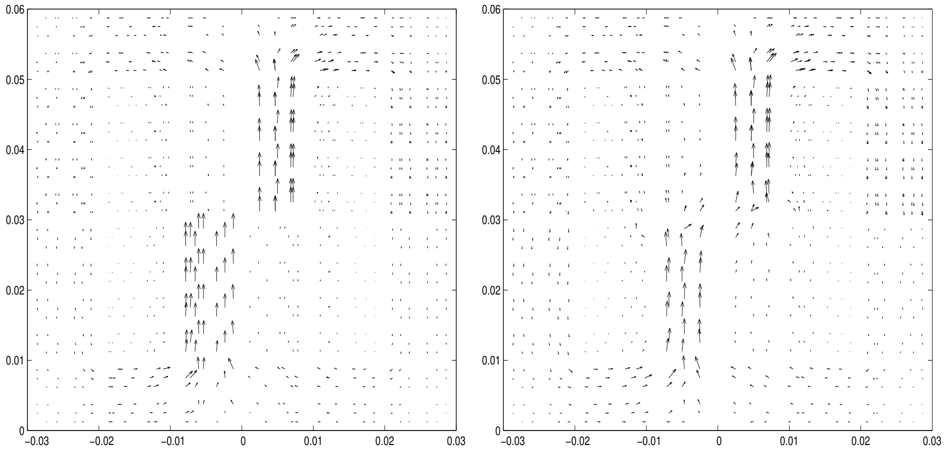

FIG. 14. *Magnetic induction distribution in the section $\theta = 0$ orthogonal to the cylinder basis: the lower part has rotated of* $135°$ *(left) and* $180°$ *(right) respectively around the cylinder axis.*

by means of a projection procedure based on the introduction of an independent third surface mesh; (4) the system of the discretized problem can be efficiently inverted by a preconditioned CG procedure. Numerical results confirm the theoretical ones and put in evidence the ability of the proposed method.

REFERENCES

[1] R. Albanese, G. Rubinacci, *Magnetostatic field computations in terms of two-component vector potentials*, Int. J. Num. Meth. in Eng., 29 (1990), pp. 515–532.

[2] A. Ben Abdallah, F. Ben Belgacem, Y. Maday, *Mortaring the two-dimensional "Nédélec" finite elements for the discretization of the Maxwell equations*, technical report R99031 of the Laboratoire d'Analyse Numérique (Paris VI Univ.), M^3AS (1998), submitted.

[3] F. Ben Belgacem, A. Buffa, Y. Maday, *The mortar element method for 3D Maxwell equations: first results*, technical report R99023 of the Laboratoire d'Analyse Numérique (Paris VI Univ.), SIAM J. Numer. Anal. (2001), to appear.

[4] F. Ben Belgacem, Y. Maday, *A Spectral Element Methodology Tuned to Parallel Implementations*, Comp. Methods Applied Mech. and Eng., 116 (1994), pp. 59–67 .

[5] C. Bernardi, Y. Maday, A. Patera, *A new nonconforming approach to domain decomposition: The mortar elements method*, in Nonlinear partial differential equations and their applications, H. Brezis and J. Lions eds., Pitman (1994), pp. 13–51.

[6] O. Biro, K. Preis, K.R. Richter, *On the use of the magnetic vector potential in the nodal and edge finite element analysis of 3D magnetostatic problems*, IEEE Trans. Magn., 32 (1996), pp. 651–654.

[7] A. Bossavit, *Computational Electromagnetism: Variational Formulations, Complementarity, Edge Elements*, Academic Press, 1988.

[8] A. Bossavit, *Edge elements for magnetostatics*, Int. J. Num. Meth. in Eng., 9 (1996), pp. 19–34.

[9] A. Buffa, Y. Maday, F. Rapetti, *A sliding mesh-mortar method for a two-dimensional eddy currents model of electric engines*, technical report R99002 of the Laboratoire d'Analyse Numérique (Universite' de Paris VI), M^2AN (2001), to appear.

[10] A. Buffa, Y. Maday, F. Rapetti, *The Mortar Element Method for 3D Maxwell's equations: analysis and application to electric engines*, in the Proceedings of the 12th International Conference on Domain Decomposition, Chiba, Japan (1999).

[11] L. Cazebeau, C. Lacour, Y. Maday, *Numerical quadratures and mortar methods*, in Computational Science for the 21st Century, John Wiley & Sons (1997), pp. 119–128.

[12] P. Ciarlet, *The Finite Element Method for Elliptic Problems*, North-Holland, Amsterdam, 1978.

[13] J.L. COULOMB, *Finite element three dimensional magnetic field computation*, IEEE Trans. Magn., 17 (1981), pp. 3241–3246.
[14] B. DAVAT, Z. REN, M. LAJOIE-MAZENC, *The movement in field modeling*, IEEE Trans. Magn., 21 (1985), pp. 2296–2298.
[15] C.R.I. EMSON, C.P. RILEY, D.A. WALSH, K. UEDA, T. KUMANO, *Modelling eddy currents induced in rotating systems*, IEEE Trans. Magn., 34 (1998), pp. 2593–2596.
[16] C. GOLOVANOV, J.-L. COULOMB, Y. MARECHAL, G. MEUNIER, *3D mesh connection techniques applied to movement simulation*, IEEE Trans. Magn., 34 (1998), pp. 3359–3362.
[17] R.H.W. HOPPE, *Mortar edge element method in* $I\!R^3$, East-West J. Num. Math., 7 (1999), pp. 159–173.
[18] Y. MARECHAL, G. MEUNIER, J.L. COULOMB, H. MAGNIN, *A general purpose tool for restoring inter-element continuity*, IEEE Trans. Magn., 28 (1992), pp. 1728–1731.
[19] G. MUR, A.T. DE HOOP, *A finite-element method for computing three-dimensional electromagnetic fields in inhomogeneous media*, IEEE Trans. Magn., 19 (1985), pp. 2188–2191.
[20] J.C. NÉDÉLEC, *Mixed finite elements in* $I\!R^3$, Numer. Math., 35 (1980), pp. 315–341.
[21] J.C. NÉDÉLEC, *A new family of mixed finite elements in* $I\!R^3$, Numer. Math., 35 (1986), pp. 57–81.
[22] A. NICOLET, F. DELINCÉ, A. GENON, W. LEGROS, *Finite elements - boundary elements coupling for the movement modeling in two dimensional structures*, J. de Phys.III, 2 (1992), pp. 2035–2044.
[23] F. RAPETTI, L. SANTANDREA, F. BOUILLAULT, A. RAZEK, *Calculation of eddy currents in moving structures using a finite element method on non-matching grids*, COMPEL, 19 (2000), pp. 10–29.
[24] F. RAPETTI, *The mortar edge element method on non-matching grids for eddy current calculations in moving structures*, Int. J. Num. Meth. in Eng. (2001), to appear.
[25] F. RAPETTI, *Approximation des équations de la magnétodynamique en domaine tournant par la méthode des éléments avec joints*, PhD Thesis, Université Pierre et Marie Curie (Paris VI) (2000).
[26] A. RAZEK, J. COULOMB, M. FELLIACHI, J. SOBONNADIÈRE, *Conception of an air-gap element for dynamic analysis of the electromagnetic fields in electric machines*, IEEE Trans. Magn., 18 (1982), pp. 655–659.
[27] Z. REN, *Influence of the R.H.S. on the convergence behaviour of the curl-curl equation*, IEEE Trans. Magn., 32 (1996), pp. 1647–1650.
[28] D. RODGER, H.C. LAI, P.J. LEONARD, *Coupled elements for problems involving movement*, IEEE Trans. Magn., 26 (1990), pp. 548–550.
[29] I.J. TSUKERMAN, *Overlapping finite elements for problems with movement*, IEEE Trans. Magn., 28 (1992), pp. 2247–2249.
[30] H. WHITNEY, *Geometric Integration Theory*, Princeton University Press, 1957.